Chemical Science

ROYAL SOCIETY OF CHEMISTRY

EDGE ARTICLE

View Article Online
View Journal | View Issue

Cite this: *Chem. Sci.*, 2025, **16**, 18383

All publication charges for this article have been paid for by the Royal Society of Chemistry

A mitochondria targeted nitroreductase-sensitive self-immolative spacer as an efficient shuttle for uncharged amine-based molecules†

Laurane Michel, Vincent Steinmetz, Sophia Godel-Pastre, Philippe Durand and Arnaud Chevalier *

Received 20th May 2025
Accepted 16th July 2025

DOI: 10.1039/d5sc03665h

rsc.li/chemical-science

Mitochondria have emerged as critical therapeutic targets in a wide range of diseases. The detailed examination of this organelle, as well as the search for methods to efficiently address it, therefore, represent significant challenges. In this article, we present a simple and robust method for the functionalization of uncharged amine-based molecules to enable their intracellular transport and selective accumulation in mitochondria. To this end, we have synthesized a self-immolative spacer that is both sensitive to mitochondrial nitroreductase and incorporates a triphenylphosphonium vectorising moiety. To demonstrate the efficacy of this mitochondrial shuttling technology, we have designed, synthesized, and employed a fluorogenic probe that unambiguously validates the concept. An initial extension of this technology for therapeutic purposes is proposed through the intramitochondrial delivery of native doxorubicin, showing promising potential for overcoming drug resistance mechanisms.

Introduction

In addition to its role as the energy powerhouse of the cell, the mitochondrion is involved in the control of several cellular processes. Its dysfunction is thus connected to numerous pathologies,[1] such as cancers[2] and neurodegenerative diseases,[3] but also overweight-related diseases such as diabetes[4] and non-alcoholic fatty liver disease.[5] Very recently, mitochondrial respiratory complex IV deficiency has been identified as a potential contributor to amyotrophic lateral sclerosis (ALS),[6] a severe neurodegenerative disease, further expanding the growing list of pathologies linked to mitochondrial dysfunction. Mitochondria thus emerge as a highly relevant biological target, fully justifying the development of innovative chemical tools to probe their functions and modulate their activity. The physicochemical properties that confer on a molecule the propensity to penetrate mitochondria are reasonably well understood. Murphy demonstrated the ability of lipophilic cations to cross the polarized double membrane of mitochondria efficiently.[7] As a result, numerous molecular entities, so-called mitochondriotropic, have emerged in recent years.[8] Their conjugation to a molecule of interest is a strategy for vectorizing the latter into mitochondria, triphenylphosphonium (TPP) being the preferred mitochondriotropic moiety.[9] In this context, various strategies have been developed to prepare mitochondria-targeted analogues of existing probes or drugs. These derivatives incorporate structural modifications, involving a mitochondriotropic moiety, that enable their selective accumulation in mitochondria, thereby facilitating the visualization and study of mitochondrial structure and activity.[8–10] The aim may be either diagnostic, by observing intra-mitochondrial biochemical processes,[11] or therapeutic,[12] by delivering active compounds. However, almost all such conjugates have been formed through the formation of an irreversible linkage between the two entities. To our knowledge, except a few techniques involving encapsulation in nanostructures coated with mito-targeting groups (mitoNANO), there are only a few implementable technologies allowing both the transport and controlled release of active molecules within the mitochondria.[13]

The reported mitochondria-targeted prodrugs are activated by photoactivation,[14] GSH,[15] ROS,[16] or carboxylesterase,[17] which are also prevalent outside the mitochondria and can thus lead to non-specific release. This study was motivated by the design of a mitochondria-targeted activatable platform responsive to mitochondria-specific enzymatic activity. Such a system enables the functionalization of uncharged molecules of interest (probes and/or drugs), facilitating their targeted delivery to mitochondria and subsequent controlled release *via* an intracellular shuttling process (Fig. 1). For this, reductases are relevant activators. Reductases are key enzymatic markers of hypoxic environments, widely exploited for diagnostic imaging[18] and prodrug activation.[19] Beyond their well-established role at low oxygen levels, recent evidence highlights their significant activity within mitochondria even under

Université Paris-Saclay, CNRS, Institut de Chimie des Substances Naturelles, UPR 2301, Gif-sur-Yvette, 91198, France. E-mail: arnaud.chevalier@cnrs.fr

† Electronic supplementary information (ESI) available. See DOI: https://doi.org/10.1039/d5sc03665h

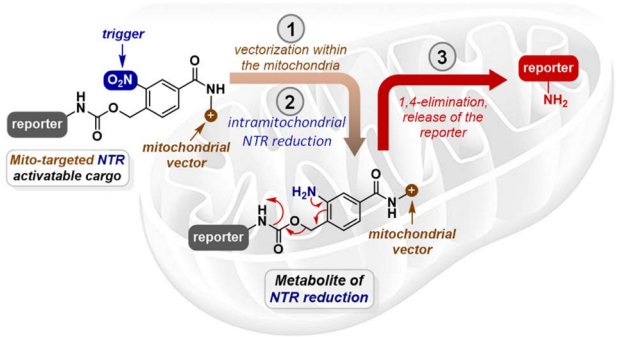

Fig. 1 Concept of "mitochondrial shuttling" using mito-targeted SIS activatable by mitochondrial NTR.

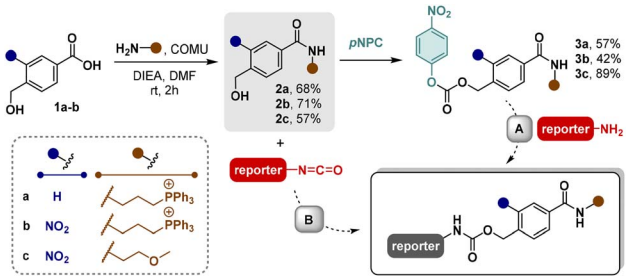

Scheme 1 Synthesis of mito-targeted NTR activatable SIS and illustration of potential use for the preparation of mito-targeted probes and/or prodrugs.

normoxic conditions. In this organelle, reductases contribute critically to maintaining redox balance, thus ensuring mitochondrial homeostasis and supporting essential bioenergetic functions.[20] This dual behavior underscores their value as both biological targets and tools for selective activation strategies within the mitochondrial microenvironment. Indeed, their selective activity within mitochondria under normoxic conditions confers a level of specificity that surpasses that of more commonly investigated biomarkers such as carboxylesterases, reactive oxygen species (ROS), or glutathione (GSH), which often lack subcellular selectivity. During the last decade, the use of fluorogenic probes has enabled the visualization of some of these intramitochondrial redox enzymes, such as thioredoxin reductases,[21] nitroreductase (NTR),[22] quinone reductases (NQOs),[23] methionine reductases (MSr)[24] and more recently azoreductase (AzoR).[25] Despite the diagnostic potential of these reductases, their use in a therapeutic context remains largely underexplored. Nonetheless, it seems obvious that they can be strategically leveraged to activate prodrugs through a controlled mitochondrial release mechanism. In this work, we introduce a novel concept: the design and synthesis of a nitroreductase-activated self-immolative spacer (SIS) bearing a triphenylphosphonium (TPP) targeting group. This SIS system enables the targeted delivery and controlled release of uncharged amine-containing molecules, including potential therapeutic agents, specifically within the mitochondria. This approach features a new paradigm in intracellular drug delivery, here called "mitochondrial shuttling" (Fig. 1). This strategy goes beyond passive covalent and permanent targeting approaches by using enzyme-triggered activation to achieve spatiotemporal control, thus marking a step forward in mitochondrial-controlled release. To our knowledge, this strategy is the first method using specific mitochondrial enzymatic activity for shuttling neutral molecules into mitochondria.

Results and discussion

Design and synthesis of mito-targeted SIS activatable by mitochondrial NTR

As illustrated in Scheme 1, the design of this self-immolative spacer (SIS) combines a mitochondriotropic triphenylphosphonium (TPP) unit with a nitro-activatable group strategically positioned in *ortho* to a benzylic alcohol. This configuration enables subsequent acylation to form carbamates from amine-based molecules of interest. To access these compounds, we developed a divergent strategy from benzylic alcohols **2ac**, relying on two complementary approaches (routes A and B) designed to accommodate both aromatic and aliphatic amines, which differ in their nucleophilicity. Here, route A involves the addition of a nucleophilic amine to a nitrophenyl carbonate (**3a–c**), while route B exploits the addition of alcohol onto an isocyanate as an activated form of less nucleophilic aniline. To enable a comprehensive study, we synthesized three analogues of each benzylic alcohol.

Compound **2a** lacks the nitro group and will serve in the synthesis of mitochondria-targeted compounds that are not activatable by nitroreductase (unactivatable control molecules). The 2-methoxy-ethyl benzamide **2c**, on the other hand, allows the generation of NTR-activatable compounds, that are not targeted to mitochondria, thereby helping to confirm the organelle selectivity of the activation process. Finally, alcohol **2b** combines both the TPP moiety and the nitro group, enabling both mitochondrial targeting and triggered release of the molecule of interest. These *para*-hydroxymethyl benzamides **2a–c** were obtained from the corresponding benzoates (**1a–b**) by an amidation reaction with amines using oxyma-based COMU as a coupling agent. The reaction with TPP carrying propyl amine led to alcohols **2a** and **2b** in 68% and 71% yield, respectively while the reaction with 2-methoxy-ethylamine led to compound **2c** in 57% yield. All the alcohols **2a–c** thus obtained were then converted to the corresponding nitrophenyl carbonates **3a–c** by reaction with *para*-nitrophenyl chloroformate (*p*NPC). All these intermediates demonstrated sufficient stability to be stored for several months under an inert atmosphere at low temperature, making them valuable and versatile tools for the single-step functionalization of a broad range of amines.

Synthesis and *in vitro* study of a fluorogenic probe incorporating the mito-targeted SIS activatable by NTR

To demonstrate the effectiveness of the shuttling process, we first used fluorescent amines that could be easily observed in cells. This fluorescent reporter was chosen to easily differentiate it from its acylated form, allowing us to confirm that the release of the reporter had occurred. To this end, 4-amino-1,8-naphthalimide (**4-ANI**) was selected as a suitable candidate

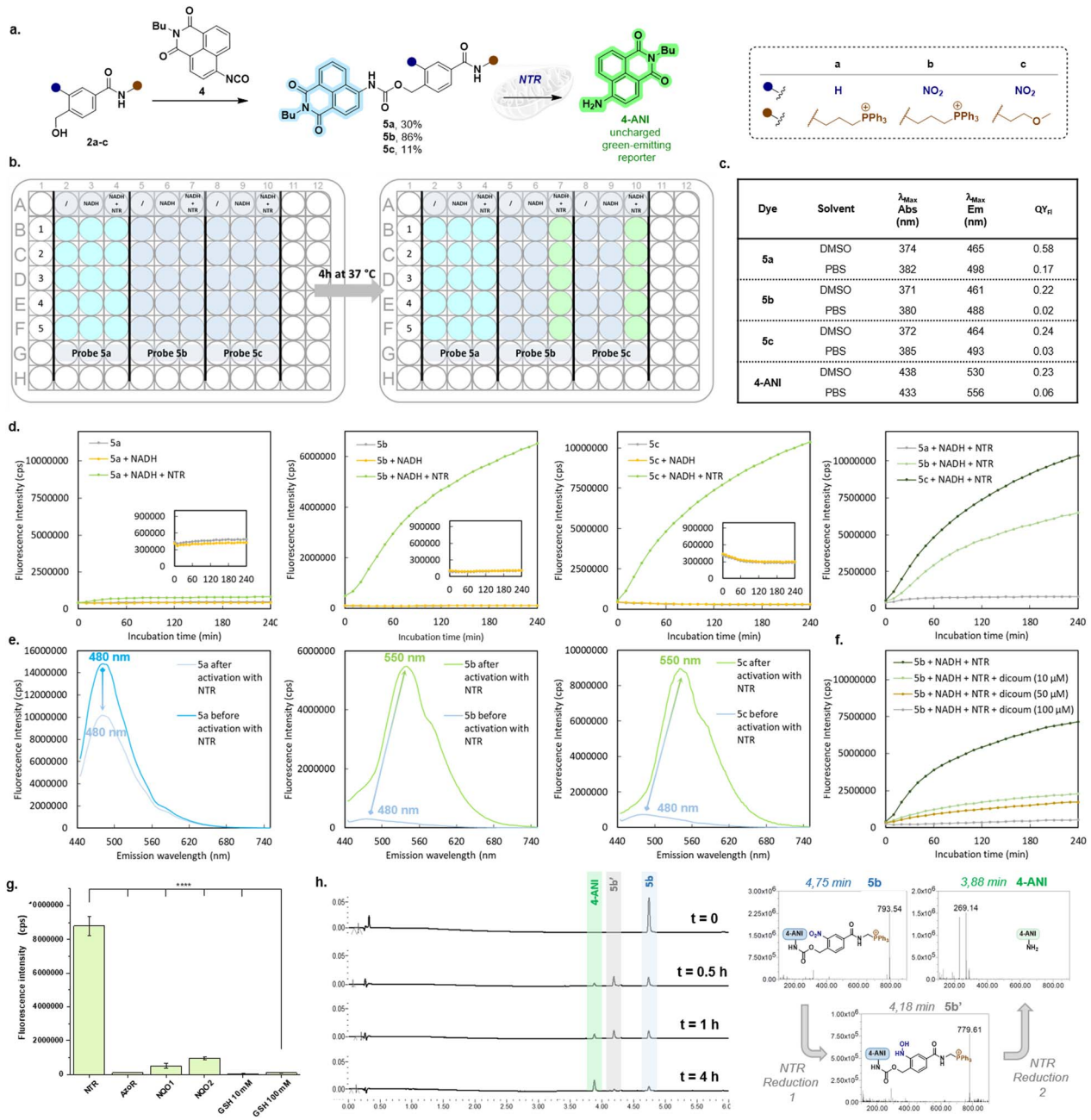

Dye	Solvent	λ_{Max} Abs (nm)	λ_{Max} Em (nm)	QY_{Fl}
5a	DMSO	374	465	0.58
	PBS	382	498	0.17
5b	DMSO	371	461	0.22
	PBS	380	488	0.02
5c	DMSO	372	464	0.24
	PBS	385	493	0.03
4-ANI	DMSO	438	530	0.23
	PBS	433	556	0.06

Fig. 2 Synthesis, photophysical characterization and *in vitro* enzymatic conversion of ratiometric fluorogenic probes **5a–c**. (a) Synthesis of a **4-ANI**-based fluorogenic probe (**5a–c**) and principle of ratiometric response to NTR. (b) Schematic representation of a 96-well plate illustrating the fluorescence emission color change associated with the release of **4-ANI** following the enzymatic activation of probes **5a–c**. (c) Photophysical properties of probes **5a–c** and **4-ANI** measured in PBS buffer and DMSO at 25 °C. Relative QY_{Fl} were calculated using quinine sulfate ($QY_{Fl} = 0.59$ in $HClO_4$ 0.1 M)[28] for probes **5a–c** or coumarin 153 ($QY_{Fl} = 0.53$ in EtOH)[28] for **4-ANI**. (d) Kinetic monitoring of NTR activation (1 µg) of probes **5a–c** (10 µM in PB buffer pH = 7.4 + NADH 500 µM). The fluorescence was recorded over time at 540 nm with excitation fixed at 435 nm. (e) Emission spectra of probes **5a–c** upon excitation at 405 nm recorded before and after incubation for 4 h with NTR in the presence of NADH (500 µM). (f) Inhibition effect of dicoumarol on **5b** activation by NTR (fluorescence was recorded over time at 540 nm with excitation fixed at 430 nm). (g) Comparison of fluorescence intensity recorded after 30 min of incubation with multiple reducing agents at 37 °C. (h) UHPLC/MS analysis of the NTR-mediated transformation of probe **5c**, giving the corresponding fluorophore **4-ANI** through the hydroxylamine intermediate **5b′** and corresponding MS spectra.

due to its well-established fluorescent properties and compatibility with acylation strategies. This fluorophore is commonly used to engineer suitable probes for fluorescence microscopy[26] including ratiometric probes.[27] Probes **5a–c** were synthesized using route B from alcohols **2a–c** and isocyanate **4**, produced *in situ* by reacting **4-ANI** with triphosgene (Fig. 2a).

Absorbance and fluorescence measurements were carried out in DMSO and PBS, and the results are shown in the table in Fig. 2c

(detailed photophysical properties are available in Table S1 and Fig. S1–S3†). They confirm that probes **5a–c** exhibit blue emission centered around 465 nm in DMSO and 490 nm in PBS. These emissions are readily distinguishable from the green emission of the expected released fluorophore, **4-ANI**, which displays maxima at 530 nm and 556 nm, respectively. Notably, the fluorescence quantum yields (QY_{Fl}) of probes **5b** and **5c** were significantly lower than that of **5a**, likely due to the photo-induced electron transfer (PeT) quenching effect arising from the nitro moiety. To assess whether the probes **5b** and **5c** could be enzymatically activated by NTR and promote the release of **4-ANI**, *in vitro* studies were performed using a commercially available enzyme. Each probe was incubated in phosphate buffer (pH 7.5) containing 1% DMSO at 37 °C. For each compound, three conditions were tested: incubation alone, with NADH, and with both NADH and NTR. Fluorescence was monitored over 4 hours using a plate reader, with each experiment performed in quintuplicate (Fig. 2b). Emission spectra were recorded before and after enzymatic activation for all probes. The release of **4-ANI** was monitored by tracking the increase in its green fluorescence at 540 nm over time, upon excitation at 435 nm (Fig. 2d). For each probe, no significant change in fluorescence was observed when incubated alone or in the presence of 500 μM NADH, confirming their stability under the experimental conditions. In contrast, a marked fluorescence increase was detected for both nitro functionalized probes **5b** and **5c** upon incubation with NTR, suggesting successful activation *via* nitro group reduction followed by the release of **4-ANI**. This was further supported by the absence of fluorescence increase for probe **5a**, which lacks the nitro-activatable moiety. Comparison of fluorescence kinetics (Fig. 2d, right, Fig. S5†) indicates that probe **5c** ($K_m = 2.72$ μM, $V_{max} = 702$ cps s^{-1}) is activated more rapidly than **5b** ($K_m = 1.98$ μM, $V_{max} = 566$ cps s^{-1}), likely due to reduced steric hindrance in the absence of the TPP moiety, which may obstruct enzyme accessibility. These findings were corroborated by emission spectra recorded before and after NTR activation (Fig. 2e). While probe **5a** showed no spectral shift, probes **5b** and **5c** exhibited a clear red shift and a pronounced fluorescence enhancement, consistent with the release of free **4-ANI**. Additionally, the fluorescence increase at 540 nm observed upon incubation of probe **5b** with NTR was progressively attenuated in the presence of increasing concentrations of dicoumarol, a known nitroreductase inhibitor (Fig. 2f), thus confirming enzyme involvement. Probe **5b** conversion was also studied in the presence of various other endogenous reducing agents, including reductases such as AzoR and NQO-1/2, as well as high concentrations of glutathione (GSH) representative of intracellular conditions (Fig. 2g and S4†). Only a slight fluorescence increase was detected in the presence of NQO-1 and NQO-2, which is consistent with their weak but known nitro-reducing activity reported in the literature.[29] Overall, these results support the selectivity of probe **5b** for NTR. Finally, UPLC-MS monitoring of the incubation of probe **5b** in the presence of NADH and NTR (Fig. 2h) confirmed the release of **4-ANI** and revealed the transient formation of the corresponding hydroxylamine intermediate (**5b′**), validating the proposed two-step NTR-mediated activation mechanism. Together, these data validate the functionality of the fluorogenic system designed for monitoring nitroreductase activity, demonstrating its ability to reliably track the enzymatic triggered release of an uncharged molecule. These promising results prompted us to pursue the study *in cellulo*, performing microscopy experiments.

Confocal imaging assessment of SIS-mediated intramitochondrial delivery of uncharged amine compounds

The probes **5a–c** were incubated for 3 h with A549 cells at a concentration of 5 μM and co-cultured in the presence of a mitochondrial near-infrared (NIR) marker.

Confocal microscopy imaging was performed in two separate channels, the settings being adjusted to give the best possible discrimination between the unactivated probe in blue and released **4-ANI** in green. As can be seen in Fig. 3a, only a blue emission was detected for probes **5a** and **5c**, indicating that no **4-ANI** release had occurred. In contrast, probe **5b** generated a distinct green signal, consistent with the release of **4-ANI**. TPP bearing probes **5a** and **5b** both displayed strong colocalization with that of the mitochondrial marker, as evidenced by Pearson correlation coefficients of 0.81 and 0.82, respectively. By comparison, the detected signal upon probe **5c** incubation showed weak colocalization (Pearson coefficient = 0.57), confirming that this control compound, which lacks the mitochondrial targeting moiety, does not accumulate in mitochondria. These data demonstrate the necessity of combining both the mitochondriotropic group and the nitro-based activation trigger to achieve efficient mitochondrial delivery of uncharged amine-containing molecules such as **4-ANI**. To undoubtedly confirm this statement, in-cell emission spectra of the three probes were recorded following excitation at 405 nm and compared to that of free **4-ANI** (Fig. 3b and S6†). Probes **5a** and **5c** displayed emission maxima estimated at 465 nm and 470 nm respectively. In contrast, probe **5b** showed a red-shifted emission centered at 510 nm, closely matching the 515 nm peak observed for **4-ANI**, thereby confirming intramitochondrial release of the fluorophore. Furthermore, treatment with dicoumarol, a known nitroreductase inhibitor, suppressed the release, resulting in a shift of the emission peak back to 475 nm (Fig. 3c and d). Finally, we recorded several images over time. While there is no doubt that the detected fluorescence upon probe **5b** incubation, attributed to the released **4-ANI**, was localized inside the mitochondria in the short time frame (Fig. 3a), it progressively spread outside the mitochondria over time and was predominantly localized in the cytosol after 8 hours of incubation (Fig. S7†). This result is consistent with the release of an uncharged molecule, which can therefore diffuse out of the mitochondria over time. Altogether, these results demonstrate that functionalizing the uncharged fluorophore **4-ANI** with the NTR-responsive, mitochondria-targeted SIS in probe **5b** enabled its efficient and selective shuttling through the cytosol to the mitochondria. To the best of our knowledge, this marks the first demonstration of a mitochondrial delivery strategy of uncharged molecules based on NTR mediated activation. We believe that this approach could be extended to a broad range of bioactive compounds, including therapeutic agents. To support this

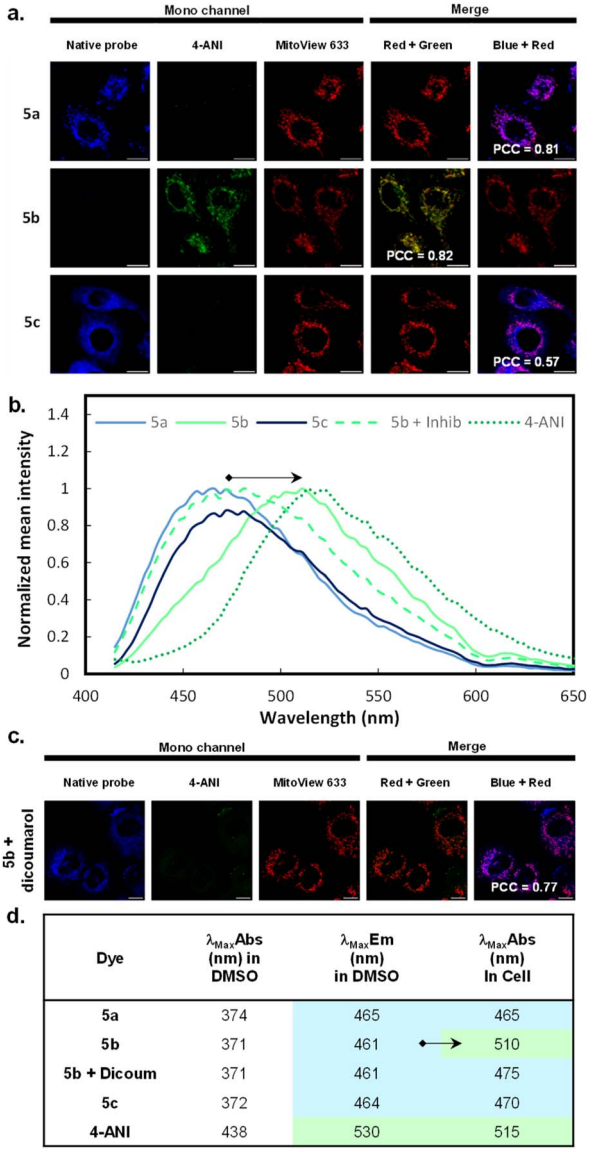

d.

Dye	λ_{Max}Abs (nm) in DMSO	λ_{Max}Em (nm) in DMSO	λ_{Max}Abs (nm) In Cell
5a	374	465	465
5b	371	461	510
5b + Dicoum	371	461	475
5c	372	464	470
4-ANI	438	530	515

Fig. 3 Confocal microscopy. (a) A549 live cells were incubated for 3 h with probes **5a–c** at 5 μM, then in the presence of MitoView 633 at 0.1 μM for 15 min. Blue: λ_{Exc}: 405 nm, λ_{Em}: 415–450 nm; green: λ_{Exc}: 440 nm, λ_{Em}: 500–550 nm. Red: λ_{Exc}: 630 nm, λ_{Em}: 650–750 nm. Pearson Correlation Coefficients (PCC) were calculated using the JAcOP plugin of ImageJ. Scale bar = 20 μm. (b) Emission spectra recorded *in cellulo* (*cf.* Fig. S4†). (c) A549 live cells were pre-incubated for 4 h with dicoumarol at 100 μM and then with probe **5b** at 5 μM for 3 h, and finally with MitoView 633 at 0.1 μM for 15 min. Blue: λ_{Exc}: 405 nm, λ_{Em}: 415–450 nm; green: λ_{Exc}: 440 nm, λ_{Em}: 500–550 nm. Red: λ_{Exc}: 630 nm, λ_{Em}: 650–750 nm. Pearson Correlation Coefficients (PCC) were calculated using the JAcOP plugin of ImageJ. Scale bar = 20 μm. (d) Absorption and emission maxima of probes **5a–c** in PBS buffer and estimated values in living cells.

potential, we applied our system to achieve the mitochondrial shuttling of doxorubicin as a first proof of concept.

Mitochondrial shuttling of doxorubicin using one-step functionalization with mitotargeted NTR activatable SIS

Prior studies, using covalent analogues of doxorubicin, have demonstrated the real relevance of targeting this drug to the

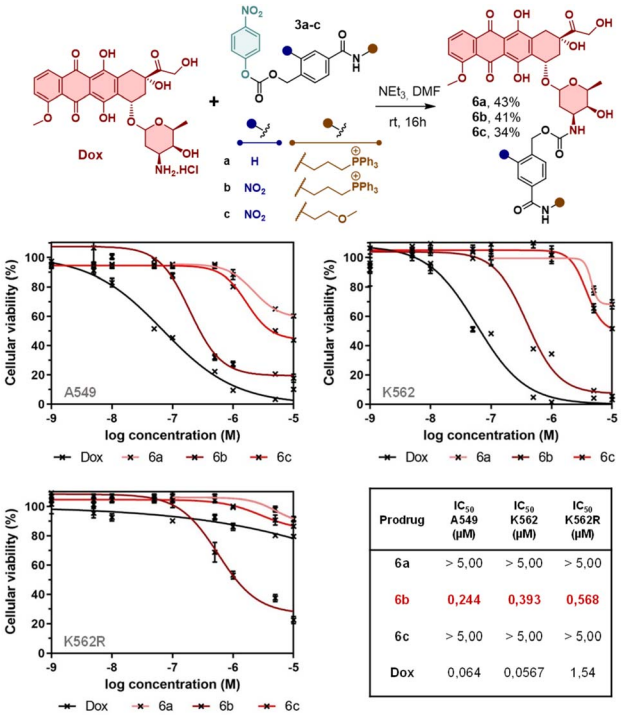

Prodrug	IC_{50} A549 (μM)	IC_{50} K562 (μM)	IC_{50} K562R (μM)
6a	> 5,00	> 5,00	> 5,00
6b	0,244	0,393	0,568
6c	> 5,00	> 5,00	> 5,00
Dox	0,064	0,0567	1,54

Fig. 4 Cell viability studies in the presence of prodrugs **6a–c** and free doxorubicin. Top: Synthesis of prodrugs **6a–c**. Bottom: Evaluation of cytotoxic activities and IC_{50} values resulting from cell viability assays performed on A549, K562 and K562r cell lines.

mitochondria for the treatment of cancer, notably by limiting nuclear effects associated with cardiotoxicity,[30] or to overcome specific resistance mechanisms.[31] In this context, we synthesized mito-targeted prodrugs of doxorubicin. Compounds **6a–c** were obtained in a single step through carbamoylation of the amine of **Dox** using nitrophenyl carbonates **3a–c** (Fig. 4).

UPLC/MS analysis of prodrug **6b** after incubation with NTR for 2 hours confirmed the formation of free doxorubicin, along with the detection of a hydroxylamine intermediate and residual **6b**. These findings point to a slower enzymatic activation compared to probe **5b** (Fig. S8†), yet they demonstrate the functional integrity of the release system. Despite our attempts to visualize compounds **6a–c** by fluorescence microscopy, no detectable signal was observed, preventing subcellular localization analysis (Fig. S9†). This limitation is most likely due to the poor intrinsic fluorescence properties of the prodrugs, as evidenced by their very low quantum yields (Fig. S10†). To assess the biological relevance of this strategy, we performed a preliminary cytotoxicity study of both prodrugs **6a–c** and native doxorubicin (**Dox**) on three different cell lines: A549, K562, and doxorubicin-resistant K562r, overexpressing P-glycoprotein (PGP) pumps. Cytotoxicity was observed for both **Dox** and prodrug **6b** on A549 and K562 cells with IC_{50} of 0.24 μM and 0.39 μM, respectively, for the latter, almost one order higher than **Dox** (Fig. 4). In the meantime, neither compounds **6a** or **6c** displayed any significant toxicity (above 5 μM). These results tend to support the requirement of both targeting and enzymatic activation, leading to intramitochondrial **Dox** release, for

a biological effect. More interestingly, while the activity of **Dox** was almost entirely lost on K562r, with IC50 rising from 0.056 μM to 1.54 μM, that of mitochondria-shuttled prodrug **6b** remained relatively constant at the submicromolar level. These results suggest that mitochondrial delivery using this mitotargeted NTR activatable SIS can bypass classical drug resistance mechanisms. Taken together, these data validate the potential of this mitochondrial shuttling strategy to enhance drug delivery, opening new avenues for its application beyond fluorophores to include therapeutic agents.

Conclusion

In summary, we report a straightforward and versatile strategy for the one-step functionalization of uncharged amine-containing molecules using a mitochondria-targeted, NTR-responsive self-immolative spacer (SIS). This approach enables efficient intracellular trafficking and selective mitochondrial delivery of uncharged amines, including both aliphatic and aromatic derivatives. The robustness of this system was first demonstrated both *in vitro* and *in cellulo* using fluorogenic probes based on the neutral dye **4-ANI**, confirming its stability, specificity, and enzymatic responsiveness. More importantly, we extended the concept to the mitochondrial delivery of doxorubicin, showing not only successful release but also preserved cytotoxic activity, even against drug-resistant cancer cells. These findings highlight the potential of this shuttling strategy to overcome resistance mechanisms commonly associated with chemotherapeutic failure. Overall, this technology represents a promising and adaptable platform for targeted mitochondrial delivery, with broad applicability in drug delivery, imaging, and therapeutic development.

Data availability

The data supporting this article, including detailed synthetic protocols, additional figures, absorbance and fluorescence spectra, NMR spectra and HRMS spectra, have been included as part of the ESI.†

Author contributions

Chemical synthesis, cell culture and related experiments including toxicity studies and confocal microscopy were performed by L. M. HPLC analysis and extraction of both chromatograms and spectra for figures were carried out by V. S. Treatment of kinetic data was performed by S. G.-P. A. C. supervised the project and wrote the manuscript, with proof reading and suggestions given by P. D. All authors have provided corrections and given approval to the final version of the manuscript.

Conflicts of interest

There are no conflicts to declare.

Acknowledgements

This project has received funding from the French National Research Agency under the program ANR-21-CE18-0005-01 grant. We also thank the Institut de Chimie des Substances Naturelles for their financial support. The present work has benefited from the Imagerie-Gif light microscopy core facility supported by the French National Research Agency (ANR-11-EQPX-0029/Morphoscope, ANR-10-INBS-04/FranceBioImaging; ANR-11-IDEX-0003-02/Saclay Plant Sciences). Laurie Askenatzis, Jérôme Bignon, Hélène Lévaique, and Emilie Mérour from the CIBI screening platform are acknowledged for their technical support. Université Paris-Saclay and the CNRS are also acknowledged.

Notes and references

1 (*a*) X. Guo, N. Yang, W. Ji, H. Zhang, X. Dong, Z. Zhou, L. Li, H.-M. Shen, S. Q. Yao and W. Huang, *Adv. Mater.*, 2021, **33**, 2007778; (*b*) M. P. Murphy and R. C. Hartley, *Nat. Rev. Drug Discovery*, 2018, **17**, 865–886.

2 (*a*) A. D. Scheid, T. C. Beadnell and D. R. Welch, *Br. J. Cancer*, 2021, **124**, 124–135; (*b*) M. Golpich, E. Amini, Z. Mohamed, R. Azman Ali, N. Mohamed Ibrahim and A. Ahmadiani, *CNS Neurosci. Ther.*, 2017, **23**, 5–22; (*c*) S. Vyas, E. Zaganjor and M. C. Haigis, *Cell*, 2016, **166**, 555–566; (*d*) D. C. Wallace, *Nat. Rev. Cancer*, 2012, **12**, 685–698; (*e*) S. Fulda, L. Galluzzi and G. Kroemer, *Nat. Rev. Drug Discovery*, 2010, **9**, 447–464.

3 (*a*) M. M. Klemmensen, S. H. Borrowman, C. Pearce, B. Pyles and B. Chandra, *Neurotherapeutics*, 2024, **21**, e00292; (*b*) G. Monzio Compagnoni, A. Di Fonzo, S. Corti, G. P. Comi, N. Bresolin and E. Masliah, *Mol. Neurobiol.*, 2020, **57**, 2959–2980; (*c*) Y. Wang, E. Xu, P. R. Musich and F. Lin, *CNS Neurosci. Ther.*, 2019, **25**, 816–824; (*d*) M. T. Lin and M. F. Beal, *Nature*, 2006, **443**, 787–795.

4 (*a*) J. Szendroedi, E. Phielix and M. Roden, *Nat. Rev. Endocrinol.*, 2011, **8**, 92–103; (*b*) B. L. Bradford and I. S. Gerald, *Science*, 2004, **303**, 1439.

5 (*a*) B. Fromenty and M. Roden, *J. Hepatol.*, 2023, **78**, 415–429; (*b*) M. Myint, F. Oppedisano, V. De Giorgi, B.-M. Kim, F. M. Marincola, H. J. Alter and S. Nesci, *J. Transl. Med.*, 2023, **21**, 757; (*c*) Y.-f. Li, Z.-f. Xie, Q. Song and J.-y. Li, *Acta Pharmacol. Sin.*, 2022, **43**, 1141–1155.

6 M. Cheng, D. Lu, K. Li, Y. Wang, X. Tong, X. Qi, C. Yan, K. Ji, J. Wang, W. Wang, H. Lv, X. Zhang, W. Kong, J. Zhang, J. Ma, K. Li, Y. Wang, J. Feng, P. Wei, Q. Li, C. Shen, X.-D. Fu, Y. Ma and X. Zhang, *Nat. Neurosci.*, 2025, **28**, 748–756.

7 (*a*) R. A. J. Smith, C. M. Porteous, A. M. Gane and M. P. Murphy, *Proc. Natl. Acad. Sci. U. S. A.*, 2003, **100**, 5407–5412; (*b*) M. P. Murphy, *Trends Biotechnol.*, 1997, **15**, 326–330.

8 S. Rin Jean, D. V. Tulumello, S. P. Wisnovsky, E. K. Lei, M. P. Pereira and S. O. Kelley, *ACS Chem. Biol.*, 2014, **9**, 323–333.

9 J. Zielonka, J. Joseph, A. Sikora, M. Hardy, O. Ouari, J. Vasquez-Vivar, G. Cheng, M. Lopez and B. Kalyanaraman, *Chem. Rev.*, 2017, **117**, 10043–10120.

10 H. Wang, B. Fang, B. Peng, L. Wang, Y. Xue, H. Bai, S. Lu, N. H. Voelcker, L. Li, L. Fu and W. Huang, *Front. Chem.*, 2021, **9**, 683220.

11 (*a*) H. Crawford, M. Dimitriadi, J. Bassin, M. T. Cook, T. F. Abelha and J. Calvo-Castro, *Chem.–Eur. J.*, 2022, **28**, e202202366; (*b*) S. Samanta, Y. He, A. Sharma, J. Kim, W. Pan, Z. Yang, J. Li, W. Yan, L. Liu, J. Qu and J. S. Kim, *Chem*, 2019, **5**, 1697–1726; (*c*) S. Wisnovsky, E. K. Lei, S. R. Jean and S. O. Kelley, *Cell Chem. Biol.*, 2016, **23**, 917–927; (*d*) Z. Xu and L. Xu, *Chem. Commun.*, 2016, **52**, 1094–1119; (*e*) Roopa, N. Kumar, V. Bhalla and M. Kumar, *Chem. Commun.*, 2015, **51**, 15614–15628.

12 (*a*) C. Ma, F. Xia and S. O. Kelley, *Bioconjugate Chem.*, 2020, **31**, 2650–2667; (*b*) J. Y. Wang, J. Q. Li, Y. M. Xiao, B. Fu and Z. H. Qin, *ChemMedChem*, 2020, **15**, 404–410.

13 (*a*) W. Zhang, G. Chen, Z. Chen, X. Yang, B. Zhang, S. Wang, Z. Li, Y. Yang, Y. Wu, Z. Liu and Z. Yu, *J. Controlled Release*, 2024, **371**, 470–483; (*b*) Y. Li, J. Liu, R. R. Weichselbaum and W. Lin, *Adv. Sci.*, 2024, **11**, 2403520; (*c*) S. S. Liew, X. Qin, J. Zhou, L. Li, W. Huang and S. Q. Yao, *Angew Chem. Int. Ed. Engl.*, 2021, **60**, 2232–2256; (*d*) T. A. Tabish and M. R. Hamblin, *Biomater. Biosyst.*, 2021, **3**, 100023; (*e*) W. Zhang, X. Hu, Q. Shen and D. Xing, *Nat. Commun.*, 2019, **10**, 1704.

14 R. Tiwari, P. S. Shinde, S. Sreedharan, A. K. Dey, K. A. Vallis, S. B. Mhaske, S. K. Pramanik and A. Das, *Chem. Sci.*, 2021, **12**, 2667–2673.

15 X. Luo, X. Gong, L. Su, H. Lin, Z. Yang, X. Yan and J. Gao, *Angew Chem. Int. Ed. Engl.*, 2021, **60**, 1403–1410.

16 H.-W. Liu, X.-X. Hu, K. Li, Y. Liu, Q. Rong, L. Zhu, L. Yuan, F.-L. Qu, X.-B. Zhang and W. Tan, *Chem. Sci.*, 2017, **8**, 7689–7695.

17 A. Sharma, M.-G. Lee, H. Shi, M. Won, J. F. Arambula, J. L. Sessler, J. Y. Lee, S.-G. Chi and J. S. Kim, *Chem*, 2018, **4**, 2370–2383.

18 J.-n. Liu, W. Bu and J. Shi, *Chem. Rev.*, 2017, **117**, 6160–6224.

19 (*a*) F. W. Hunter, B. G. Wouters and W. R. Wilson, *Br. J. Cancer*, 2016, **114**, 1071–1077; (*b*) X. Yuan, Z. Xie and T. Zou, *Bioorg. Chem.*, 2024, **144**, 107161.

20 (*a*) P. Kameritsch, M. Singer, C. Nuernbergk, N. Rios, A. M. Reyes, K. Schmidt, J. Kirsch, H. Schneider, S. Müller, K. Pogoda, R. Cui, T. Kirchner, C. de Wit, B. Lange-Sperandio, U. Pohl, M. Conrad, R. Radi and H. Beck, *Proc. Natl. Acad. Sci. U. S. A.*, 2021, **118**, e1921828118; (*b*) V. Scalcon, A. Bindoli and M. P. Rigobello, *Free Radical Biol. Med.*, 2018, **127**, 62–79; (*c*) F. Cabreiro, C. R. Picot, M. Perichon, J. Castel, B. Friguet and I. Petropoulos, *J. Biol. Chem.*, 2008, **283**, 16673–16681.

21 (*a*) T. J. Mafireyi, J. O. Escobedo and R. M. Strongin, *Results Chem.*, 2021, **3**, 100127; (*b*) H.-W. Liu, S. Xu, P. Wang, X.-X. Hu, J. Zhang, L. Yuan, X.-B. Zhang and W. Tan, *Chem. Commun.*, 2016, **52**, 12330–12333; (*c*) M. H. Lee, J. H. Han, J. H. Lee, H. G. Choi, C. Kang and J. S. Kim, *J. Am. Chem. Soc.*, 2012, **134**, 17314–17319.

22 (*a*) S. Wang, W. Tan, W. Lang, H. Qian, S. Guo, L. Zhu and J. Ge, *Anal. Chem.*, 2022, **94**, 7272–7277; (*b*) M. Safir Filho, P. Dao, A. R. Martin and R. Benhida, *J. Photochem. Photobiol., A*, 2020, **396**, 112528; (*c*) N. Zhu, G. Xu, R. Wang, T. Zhu, J. Tan, X. Gu and C. Zhao, *Chem. Commun.*, 2020, **56**, 7761–7764; (*d*) Z. Thiel and P. Rivera-Fuentes, *Angew Chem. Int. Ed. Engl.*, 2019, **58**, 11474–11478; (*e*) B. Huang, W. Chen, Y. Q. Kuang, W. Liu, X. J. Liu, L. J. Tang and J. H. Jiang, *Org. Biomol. Chem.*, 2017, **15**, 4383–4389; (*f*) A. Chevalier, Y. Zhang, O. M. Khdour, J. B. Kaye and S. M. Hecht, *J. Am. Chem. Soc.*, 2016, **138**, 12009–12012.

23 (*a*) Y. P. Yang, F. J. Qi, Y. P. Qian, X. Z. Bao, H. C. Zhang, B. Ma, F. Dai, S. X. Zhang and B. Zhou, *Anal. Chem.*, 2021, **93**, 2385–2393; (*b*) Z. Yuan, M. Xu, T. Wu, X. Zhang, Y. Shen, U. Ernest, L. Gui, F. Wang, Q. He and H. Chen, *Talanta*, 2019, **198**, 323–329; (*c*) W. S. Shin, M. G. Lee, P. Verwilst, J. H. Lee, S. G. Chi and J. S. Kim, *Chem. Sci.*, 2016, **7**, 6050–6059.

24 M. H. Xiang, H. Huang, X. J. Liu, Z. X. Tong, C. X. Zhang, F. Wang, R. Q. Yu and J. H. Jiang, *Anal. Chem.*, 2019, **91**, 5489–5493.

25 L. Michel, M. Auvray, L. Askenatzis, M.-A. Badet-Denisot, J. Bignon, P. Durand, F. Mahuteau-Betzer and A. Chevalier, *Anal. Chem.*, 2024, **96**, 1774–1780.

26 (*a*) H. Xu, Y. Xiao, Y.-G. Liu and W. Sun, *Adv. Sens. Res.*, 2024, **3**, 2300032; (*b*) C. Geraghty, C. Wynne and R. B. P. Elmes, *Coord. Chem. Rev.*, 2021, **437**, 213713.

27 (*a*) W. Mao, X. Qian, J. Zhang, L. Xia and H. Xie, *ChemBioChem*, 2017, **18**, 1990–1994; (*b*) Q. Jin, L. Feng, D.-D. Wang, Z.-R. Dai, P. Wang, L.-W. Zou, Z.-H. Liu, J.-Y. Wang, Y. Yu, G.-B. Ge, J.-N. Cui and L. Yang, *ACS Appl. Mater. Interfaces*, 2015, **7**, 28474–28481; (*c*) L. Dong, S. Shen, H. Lu, S. Jin and J. Zhang, *ACS Sens.*, 2019, **4**, 1222–1229.

28 C. Würth, M. Grabolle, J. Pauli, M. Spieles and U. Resch-Genger, *Nat. Protoc.*, 2013, **8**, 1535–1550.

29 R. J. Knox and S. Chen, in *Methods in Enzymology*, Academic Press, 2004, vol. 382, pp. 194–221.

30 S. R. Jean, D. V. Tulumello, C. Riganti, S. U. Liyanage, A. D. Schimmer and S. O. Kelley, *ACS Chem. Biol.*, 2015, **10**, 2007–2015.

31 (*a*) J. Xi, M. Li, B. Jing, M. An, C. Yu, C. B. Pinnock, Y. Zhu, M. T. Lam and H. Liu, *ACS Appl. Mater. Interfaces*, 2018, **10**, 43482–43492; (*b*) W.-Q. Li, Z. Wang, S. Hao, H. He, Y. Wan, C. Zhu, L.-P. Sun, G. Cheng and S.-Y. Zheng, *ACS Appl. Mater. Interfaces*, 2017, **9**, 16793–16802; (*c*) Y. Zhang, C. Zhang, J. Chen, L. Liu, M. Hu, J. Li and H. Bi, *ACS Appl. Mater. Interfaces*, 2017, **9**, 25152–25163; (*d*) G. R. Chamberlain, D. V. Tulumello and S. O. Kelley, *ACS Chem. Biol.*, 2013, **8**, 1389–1395.